

A New Soft-Switched PFC Boost Rectifier with Integrated Flyback Converter for Stand-by Power

Yungtaek Jang, Dave L. Dillman, and Milan M. Jovanović

Delta Products Corporation
Power Electronics Laboratory
P.O. Box 12173, 5101 Davis Drive
Research Triangle Park, NC 27709

Abstract — The paper presents a magnetic integration approach that reduces the number of magnetic components in a power supply by integrating the some magnetic components in two conversion stages. Specifically, in the proposed approach, a single transformer is used to implement the continuous-conduction-mode boost PFC converter and the dc-dc flyback converter. The integrated boost and flyback converters offer soft switching of all semiconductor switches including a controlled di/dt turn-off rate of the boost rectifier. The performance of the proposed approach was evaluated on a 150-kHz, 450-W, universal-line range boost PFC converter with 12-V/2.2-A integrated stand-by flyback converter.

1. Introduction

The majority of today's ac-dc power supplies used in modern data processing and telecom equipment have a boost power-factor-corrected (PFC) front end and a low-power stand-by power supply. The block diagram in Fig. 1 shows the typical structure of an off-line power supply for those applications. The front-end boost rectifier is employed to reduce the line-current harmonics and to provide compliance with various worldwide specifications governing the harmonic limits of the line current in ac-dc power supplies. On the other hand, the main purpose of the stand-by power supply is to provide housekeeping power and to ensure system functionality when the system is in low-power (stand-by or sleep) mode. The majority of stand-by power supplies are implemented with a flyback converter due to its low part count and its ability to operate efficiently in a wide input-voltage range.

To meet the challenges of the ever-present requirement to decrease the size of power conversion equipment, power supplies operating at higher switching frequencies and utilizing advanced packaging and thermal management techniques have been introduced. Specifically, in recent years, significant efforts have been made to reduce switching losses of continuous-conduction-mode (CCM) boost converters since the CCM boost converter is the preferred topology for implementation of a front end with PFC over the range from medium to high power. So far, a number of soft-switched boost converters and their variations have been proposed [1] - [16]. All of them employ an auxiliary active

switch with a few passive components to form an active snubber that is used to control the di/dt rate of the rectifier current and to create conditions for zero-voltage switching (ZVS) or zero-current switching (ZCS) of the main switch.

A further size reduction can be achieved by minimizing the number of components through component integration. As already have been demonstrated, the number of components can be reduced by integrating semiconductor switches with drive, control and/or supervisory circuits and/or by integrating magnetic components such as transformers and inductors on the same core.

This paper presents a new magnetic integration approach where the reduction of the number of magnetic components in a power supply is achieved by utilizing the same magnetic component in two conversion stages of the power supply. Specifically, in the proposed approach, a single transformer is used to implement the integration of the CCM PFC boost converter and the flyback stand-by converter. The proposed magnetically integrated boost and flyback converters feature soft-switching of all semiconductors. The boost switch and the primary side flyback converter switch are turned on at zero voltage, whereas the active-snubber switch of the boost converter turns off at zero current. In addition, the boost rectifier is turned off softly with the controlled di/dt rate so that reverse-recovery-related losses of the boost rectifier are virtually eliminated.

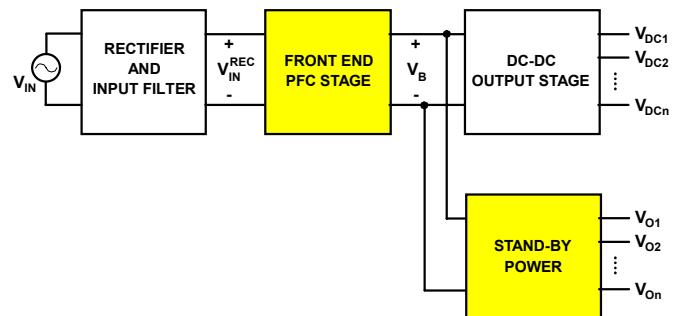


Fig. 1. Block diagram of a typical ac-dc power supply.

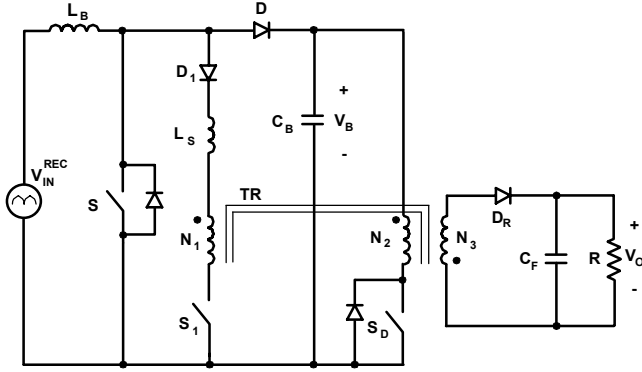


Fig. 2. Proposed soft-switched power supply that integrates a boost converter and a flyback converter.

2. Soft-Switched PFC Boost Converter with Integrated Flyback Converter

The proposed soft-switched boost converter magnetically integrated with a stand-by flyback dc-dc converter is shown in Fig. 2. The boost converter consists of voltage source V_{IN}^{REC} , boost inductor L_B , main switch S , output rectifier D , energy-storage capacitor C_B , and the active snubber circuit formed by auxiliary switch S_1 , winding N_1 of transformer TR , snubber inductor L_S , and blocking diode D_1 . The stand-by flyback converter consists of switch S_D with an associated antiparallel diode, isolation transformer TR , and the secondary side circuit that consists of rectifier D_R and output capacitor C_F .

To facilitate the explanation of the circuit operation, Fig. 3 shows a simplified circuit diagram of the proposed converter in Fig. 2. In the simplified circuit, energy-storage capacitor C_B is modeled by voltage source V_B by assuming that the value of C_B is large enough so that the voltage ripple across the capacitor is small in comparison to its dc voltage. In addition, boost inductor L_B is modeled as constant current source I_{IN} by assuming that the inductance of L_B is large so

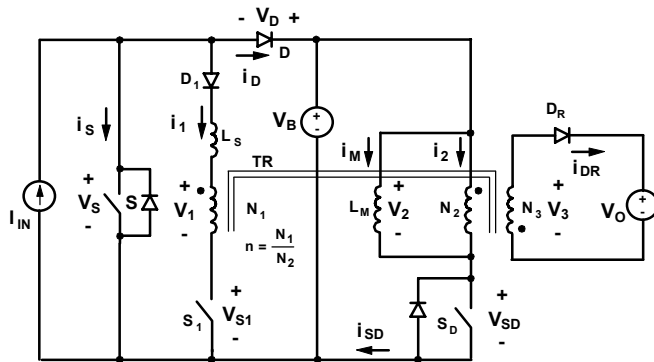


Fig. 3. Simplified circuit diagram of the proposed converter shown in Fig. 2 along with reference directions of key currents and voltages.

that during a switching cycle the current through it does not change significantly. In this analysis, the leakage inductance of the transformer is neglected since it does not have a significant effect on the operation of the circuit. Moreover, the effect of the leakage inductance on the operation of the circuit can be accounted to the effect of snubber inductor L_S since L_S is connected in series with the leakage inductance of winding N_1 . As a result, transformer TR is modeled by magnetizing inductance L_M and three-winding ideal transformer. Finally, it is assumed that in the on state, semiconductors exhibit zero resistance, *i.e.*, they are short circuits. However, the output capacitance of the switches, as well as the junction capacitance and the reverse-recovery charge of the boost rectifier are not neglected in this analysis.

To further facilitate the analysis of operation, Fig. 4 shows the major topological stages of the circuit in Fig. 2 during a switching cycle, whereas Fig. 5 shows its key waveforms. The reference directions of currents and voltages plotted in Fig. 5 are shown in Fig. 3.

As can be seen from the timing diagrams in Figs. 5(a), (b) and (c), the turn on of boost switch S and of flyback switch S_D are synchronized, whereas auxiliary switch S_1 is turned on prior to the turn on of switches S and S_D . In addition, auxiliary switch S_1 is turned off before boost switch S or flyback switch S_D is turned off, *i.e.*, the proposed circuit operates with overlapping gate drive signals for the active snubber switch and the converter switches.

Prior to the turn on of switch S_1 at $t=T_0$, all switches are open. As a result, the entire input current I_{IN} flows through boost rectifier D into energy-storage capacitor C_B in the boost power stage, while reflected magnetizing current $i_{DR}=(N_2/N_3)i_M$ flows through output rectifier D_R in the flyback power stage as shown in Fig. 4(l). Because output rectifier D_R is conducting during this period, the output voltage is induced across winding N_1 of transformer TR , *i.e.*, $v_1=-(N_1/N_3)V_O$. After switch S_1 is turned on at $t=T_0$, the voltage of energy-storage-capacitor V_B plus induced voltage $(N_1/N_3)V_O$ is applied across snubber inductor L_S so that current i_1 starts to increase linearly, as illustrated in Fig. 5(g). The slope of current i_1 is

$$\frac{di_1}{dt} = \frac{V_B - v_1}{L_S} = \frac{V_B + n_1 V_O}{L_S}, \quad (1)$$

where $n_1=N_1/N_3$.

As current i_1 starts flowing through winding N_1 of transformer TR , the current in winding N_3 starts to decrease, *i.e.*, $i_{DR}=(N_2/N_3)i_M - (N_1/N_3)i_1$, as shown in Fig. 4(a) and Fig. 5(k). Current i_{DR} decreases until it becomes zero at $t=T_1$, *i.e.*, output rectifier D_R turns off. Since the current through winding N_3 is zero after the turn-off of D_R , the increasing current in winding N_1 makes current i_2 in winding N_2 larger than magnetizing current i_M . This excessive current discharges the output capacitance of switch S_D , as illustrated in Fig. 4(b) and Fig. 5(d). During this period, voltage v_2 across winding N_2 of transformer TR starts to increase. After

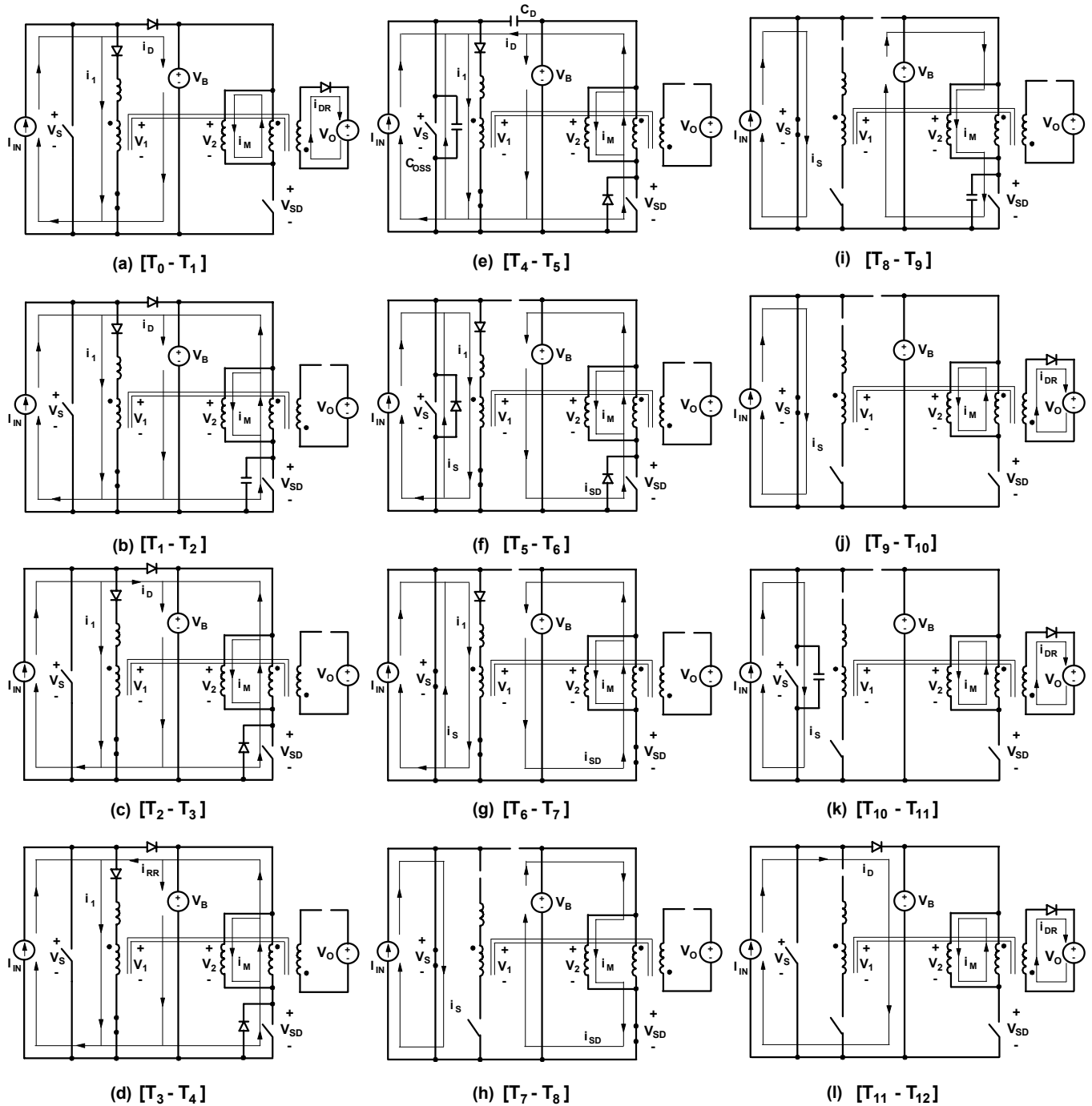


Fig. 4. Topological stages during a switching period of the proposed circuit.

the output capacitance of switch S_D is fully discharged at $t=T_2$, current i_{SD} continues to flow through the antiparallel diode of switch S_D , as shown in Fig. 4(c) and Fig. 5(i). To achieve ZVS of S_D , switch S_D should be turned on while its antiparallel diode is conducting. To simplify the control circuit timing diagram, the turn-on of switch S_D is synchronized with the turn-on of boost switch S . When the

antiparallel diode of switch S_D is conducting, voltage v_2 across winding N_2 is equal to V_B so that induced voltage v_1 on winding N_1 is

$$v_1 = \frac{N_1}{N_2} V_B = n V_B, \quad (2)$$

where it is required that turns ratio $n=N_1/N_2$ should be less than 0.5 for proper operation of the proposed circuit.

Since v_1 is constant, voltage applied across snubber inductor L_S is also constant so that current i_1 increases linearly with a slope of

$$\frac{di_1}{dt} = \frac{V_B - v_1}{L_S} = \frac{V_B - nV_B}{L_S} = (1-n) \frac{V_B}{L_S}. \quad (3)$$

During the same period, magnetizing inductance i_M increases with a slope given by

$$\frac{di_M}{dt} = \frac{V_B}{L_M}. \quad (4)$$

As current i_1 linearly increases, boost rectifier current i_D linearly decreases at the same rate since the sum of i_1 and i_D is equal to constant input current I_{IN} , *i.e.*, $i_1 + i_D = I_{IN}$. Therefore, in the proposed circuit, the turn-off rate of the boost rectifier

$$\frac{di_D}{dt} = -(1-n) \frac{V_B}{L_S} \quad (5)$$

can be controlled by the proper selection of the inductance value of snubber inductor L_S and turns ratio n of transformer TR. Typically, for today's fast-recovery rectifiers, the turn-off rate di_D/dt should be kept around 100 A/ μ s. With selected turn-off rate as such, the reverse-recovery current of the rectifier and the related power losses and EMI problems are minimized.

The topological stage in Fig. 4(c) ends at $t=T_3$ when the forward current in boost rectifier D becomes zero. Until $t=T_4$, the reverse-recovery current of boost rectifier D flows through snubber inductor L_S . After $t=T_4$, current i_1 starts to discharge the output capacitance of boost switch S and charge the junction capacitance of boost rectifier D, as shown in Fig. 4(e). If the turns ratio of transformer TR is selected so that $n < 0.5$, the energy stored in L_S is sufficient to completely discharge the output capacitance of boost switch S regardless of the load and line conditions. Once the capacitance is fully discharged at $t=T_5$, current i_S continues to flow through the antiparallel diode of boost switch S, as shown in Fig. 4(f) and Fig. 5(h). During the period when the voltage across boost switch S is zero, voltage v_1 is applied in the negative direction across snubber inductor L_S . Therefore, current i_1 starts to decrease linearly at the rate given by

$$\frac{di_1}{dt} = -\frac{nV_B}{L_S}, \quad (6)$$

as illustrated in Fig. 5(g). The current in auxiliary switch S_1 also starts to decrease, whereas boost-switch current i_S starts to increase from the negative peak value, as shown in Figs. 5(g) and (h). To achieve ZVS of boost switch S, it is necessary to turn on boost switch S before its current becomes positive at $t=T_6$, *i.e.*, during the period when current i_S still flows through the antiparallel diode of switch S, as illustrated in Fig. 5(h).

As shown in Fig. 5(g), current i_1 continues to decrease until it reaches zero at $t=T_7$. Shortly after $t=T_7$, auxiliary switch S_1 is turned off to achieve ZCS. After switch S_1 is turned off, the entire input current I_{IN} flows through boost switch S. As a

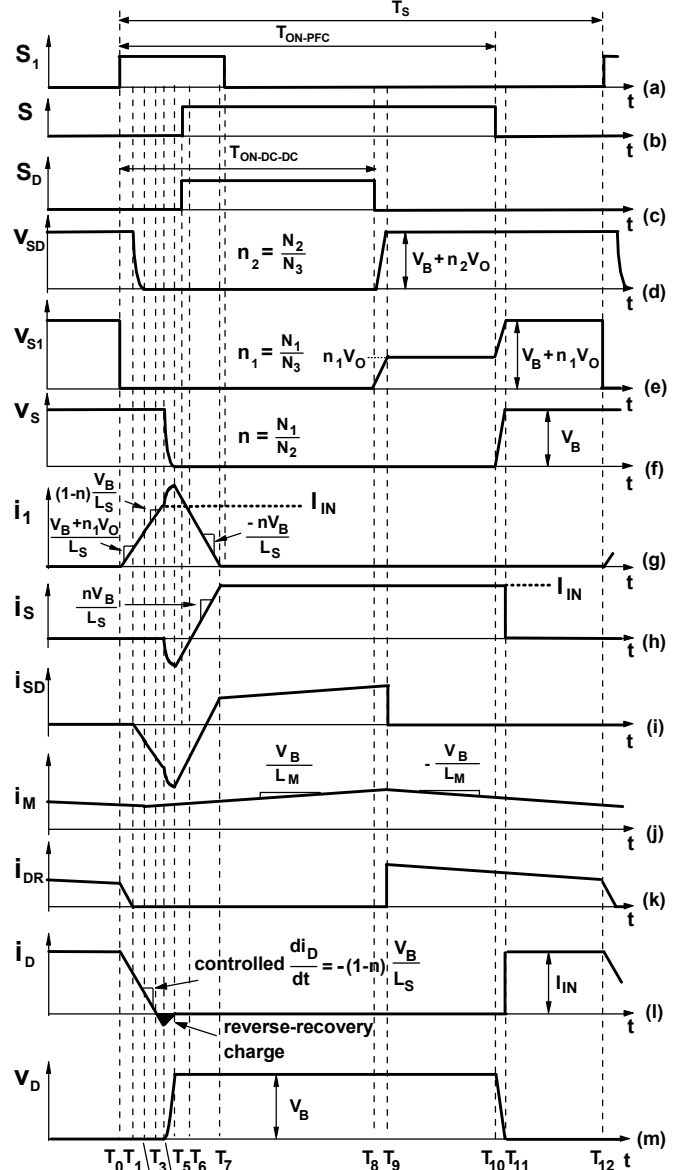


Fig. 5. Key waveforms of the proposed converter.

result, the front-end boost converter stage is completely decoupled from the stand-by flyback converter stage, as shown in Fig. 4(h). For the rest of the switching cycle, the flyback converter stage continues to operate as a conventional flyback converter.

After flyback-converter switch S_D is turned off at $t=T_8$, magnetizing current i_M start to charge the output capacitance of switch S_D , as shown in Fig. 4(i). When voltage v_{SD} reaches $V_B + n_2 V_O$ at $t=T_9$, diode D_R starts to conduct, which forces the commutation of the magnetizing current from switch S_D to output diode D_R , as shown in Fig. 4(j). At the same time, the reset of the transformer is initiated by applied output voltage

V_O across winding N_3 . During the reset time of the transformer, voltages v_{SD} across the flyback-converter switch is equal to $(N_2/N_3)V_O+V_B$, whereas the voltage across auxiliary switch S_1 is $(N_1/N_3)V_O$ due to the magnetic coupling of windings N_1 and N_2 , as illustrated in Figs. 5(d) and (e).

After boost switch S is turned off at $t=T_{10}$, voltage across switch S starts increasing linearly because constant input current I_{IN} starts charging the output capacitance of boost switch S , as shown in Fig. 4(k). The increasing boost-switch voltage causes an equal increase of voltage v_{S1} across auxiliary switch S_1 . When boost-switch voltage v_S reaches V_B at $t=T_{11}$, boost diode D begins to conduct, as shown in Fig. 4(l). At the same time, auxiliary-switch voltage v_{S1} reaches its maximum value of $(N_1/N_3)V_O+V_B$. The circuit stays in the topological stage shown in Fig. 4(l) until the next switching cycle is initiated at $t=T_{12}$.

In summary, the major feature of the proposed circuit in Fig. 2 is the soft-switching of all semiconductor devices. Specifically, boost switch S and flyback-converter switch S_D are turned on with ZVS, whereas auxiliary switch S_1 is turned off with ZCS. In addition, boost diode D is turned off with a controlled turn-off rate of its current. Because all semiconductor components of the proposed converter operates with soft switching, the overall switching losses are minimized, which maximizes the conversion efficiency. In addition, soft switching has a beneficial effect on EMI and may result in a smaller size input filter.

However, it should be noted that complete ZVS of flyback-converter switch S_D can only be achieved if input current I_{IN} (which is being commutated to winding N_1 when auxiliary switch S_1 is closed) is large enough to produce a negative current through primary winding N_2 and discharge the output capacitance of switch S_D , as shown in Fig. 4(b). According to Fig. 4(b), to have a negative current flowing through winding N_2 after $t=T_1$, reflected current i_1 in winding N_2 has to be greater than magnetizing current i_M . If this condition is not met, switch S_D operates with partial ZVS. This mode of operation typically occurs in ac-dc applications when they operate near the zero crossing of the line voltage. Since the input current is proportional to the line voltage in PFC operation, input current I_{IN} is small near the zero crossing of the line voltage.

Due to the ZVS of the boost switch and the flyback switch, the most suitable implementation of the circuit in Fig. 2 is with the boost switch and the flyback switch consisting of MOSFET (Metal Oxide Semiconductor Field Effect Transistor) devices. Similarly, due to the ZCS of auxiliary switch S_1 , an IGBT (Insulated Gate Bipolar Transistor) is suitable for the auxiliary switch.

In the proposed circuit, the voltage stresses on switches S , S_D , and boost rectifier D are identical to the corresponding stresses in the conventional boost converter without a snubber. However, the voltage stress of auxiliary switch S_1 is

$$v_{S1(MAX)} = V_B + n_1 V_O. \quad (7)$$

The control of the proposed circuit is performed by two independent controllers that are synchronized. Specifically, one controller is used to regulate the output voltage of the front-end boost stage, *i.e.*, voltage V_B across the energy-storage capacitor C_B . The other controller is used to regulate output voltage V_O of the flyback converter. Any control strategy can be used to control these two voltages, including multi-loop control strategies such as various current-mode control implementations.

3. Experimental Results

The performance of the proposed soft-switched converter was evaluated on a 450-W prototype circuit that was designed to operate from a universal ac-line input ($90 V_{RMS}$ - $264 V_{RMS}$) and deliver up to 1.2 A at 380-V output. Moreover, the integrated flyback converter delivers 26-W stand-by power at 12-V output. Switches S , S_1 , and S_D operate at 150 kHz.

Since the drain voltage of boost switch S is clamped to bulk capacitor C_B , the peak voltage stress on boost switch S is approximately 380 V. The peak current stress on switch S , which occurs at full load and low line, is approximately

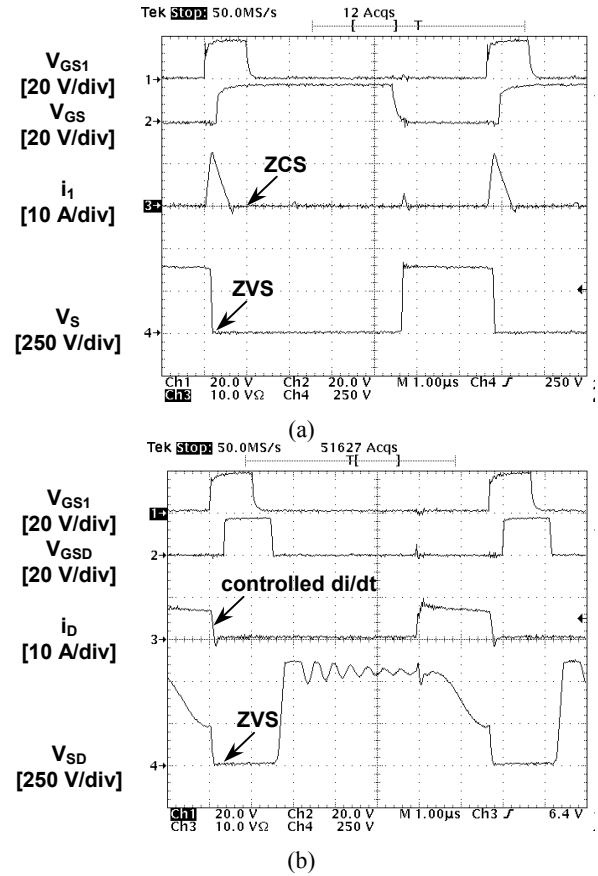


Fig. 6. Measured waveforms of the proposed circuit at $V_{IN}=90 V$, $V_B=380 V$, $V_O=12 V$, $P_{DC}=450 W$, $P_{AUX}=26 W$. Time base: 1 μ s/div.

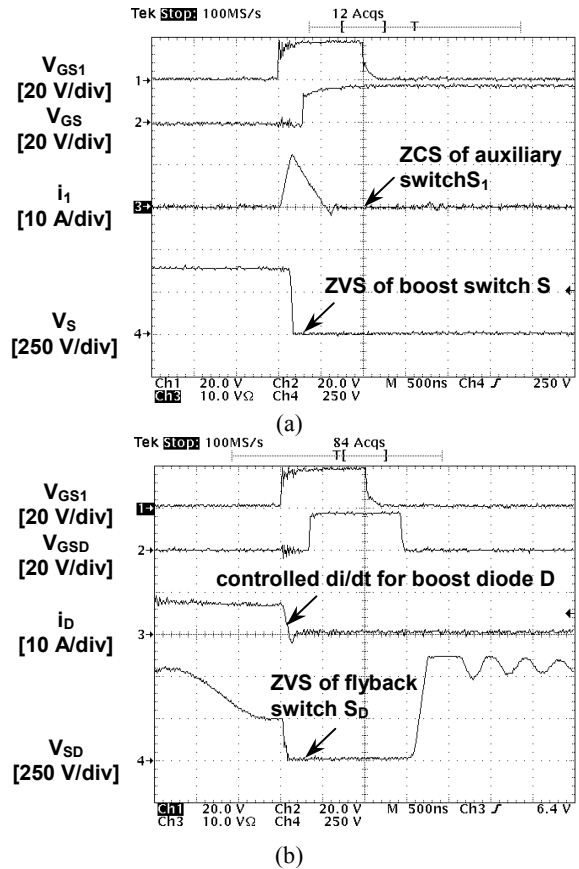


Fig. 7. Expanded waveforms shown in Fig. 6 at $V_{IN}=90$ V, $V_B=380$ V, $V_O=12$ V, $P_{DC}=450$ W, $P_{AUX}=26$ W. Time base: $0.5 \mu\text{s}/\text{div}$.

7.8 A. Therefore, an SPP20N60C2 MOSFET ($V_{DSS} = 600$ V, $I_{D25} = 20$ A, $R_{DS} = 0.19 \Omega$) from Infineon was used for the boost switch. The maximum drain voltage of flyback switch S_D is $V_{SD(MAX)} = V_B + n_2 V_O = 380 + (52/4)12$, as shown in Fig. 5(d). As a result, the peak voltage stress on flyback switch S_D is approximately 536 V. The peak current stress on flyback switch S_D is approximately 1.3 A, therefore, an SPA11N80C3 MOSFET ($V_{DSS} = 800$ V, $I_{D25} = 11$ A, $R_{DS} = 0.45 \Omega$) from Infineon was used for the flyback switch. Moreover, a high speed HGTG12N60A4 IGBT ($V_{RRM} = 600$ V, $I_F = 12$ A) from Fairchild was used as auxiliary switch S_1 since its maximum drain voltage is $V_{S1(MAX)} = V_B + n_1 V_O = 380 + (12/4)12 = 416$ V, as shown in Eq. (7).

Since boost diodes D must block the bulk voltage and must conduct the peak input current, which is approximately 7.8 A, an RHRP1560 diode ($V_{RRM} = 600$ V, $I_{FAVM} = 15$ A) from Fairchild was used as boost diode D . An RHRP860 diode ($V_{RRM} = 600$ V, $I_{FAVM} = 8$ A) was used as diode D_1 . A 16CTQ060 diode ($V_{RRM} = 60$ V, $I_{FAVM} = 16$ A) from IRF was used as output diode D_R . To reduce the conduction losses of the switches and output diodes, devices which have higher

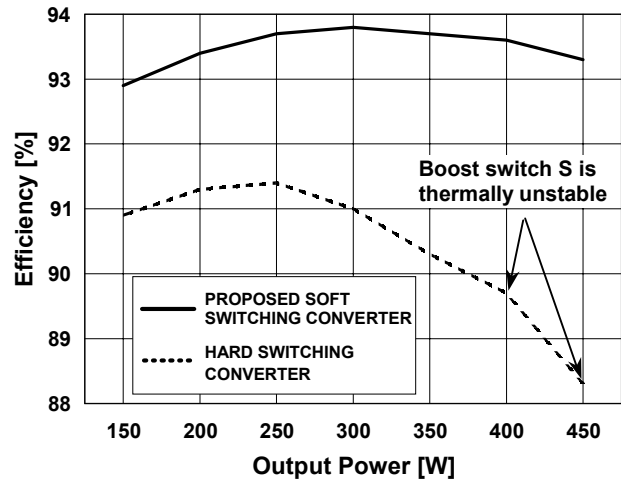


Fig. 8. Measured efficiency of the 150 kHz, 450-W experimental converter with (dashed line) hard switching and (solid line) soft switching at $V_{IN}=90$ V_{AC} and $V_B=380$ V as functions representing output power of PFC boost converter, where the integrated flyback converter supplies 26 W constant stand-by power at 12 V output voltage.

current ratings than the designed maximum current were selected.

To obtain the desired inductance of boost inductor L_B of approximately 250 μH at full load, the boost inductor was built using a toroidal core (MS130060) from Arnold and 71 turns of magnet wire (AWG #19).

External snubber inductor L_S was connected in series with winding N_1 of transformer TR , as shown in Fig. 2. The required inductance is approximately 2.4 μH at full load. Snubber inductor L_S was built using a toroidal core (A189043) from Arnold and 8 turns of magnet wire (AWG #19).

Transformer TR was built using a pair of ferrite cores (Philips, ER35-3F3) with an air gap (4 mils). Three magnet wires ($N_1=12$ turns: $N_2=52$ turns: $N_3=4$ turns) were used to obtain the desired magnetizing inductance.

A high voltage aluminum capacitor (470 μF , 450 VDC) was used for bulk capacitor C_B to meet the hold-up time requirement. A low voltage aluminum capacitor (220 μF , 16 VDC) was used for output capacitor C_F .

Figures 6 and 7 show the oscillograms of key waveforms in the experimental converter when it delivers full power from the low line input voltage. As can be seen from the corresponding waveforms in Fig. 5, there is a good agreement between the experimental and theoretical waveforms. As can be seen from Figs. 6 and 7, switches S and S_D are turned on with ZVS since their voltages V_S and V_{SD} fall to zero before gate-drive signals V_{GS} and V_{GSD} become high. Moreover, auxiliary switch S_1 achieves soft-switching turn off because switch current i_1 becomes zero before auxiliary switch S_1 is

turned off. Also, it should be noted that the slope of rectifier current i_D is approximately $di/dt = 80 \text{ A}/\mu\text{s}$ during the period when boost diode D is turned off. The rectifier-current slope is controlled by snubber inductance L_s , as indicated in Figs. 6 and 7. With this di/dt rate, peak reverse-recovery current I_{RR} is reduced to approximately 2 A.

Figure 8 shows the measured efficiencies of the experimental converter with (solid lines) and without (dashed lines) the active snubber circuit as functions representing output power of PFC front end. As can be seen in Fig. 8, the active snubber improves the conversion efficiency in the entire measured power range. The efficiency improvement is more pronounced at higher power levels where the reverse-recovery losses are greater. The active snubber improves the efficiency by approximately 5% at 450 W, which translates into approximately 50% reduction of losses.

Since all switches operate with zero-voltage or zero-current switching, the rectifier reduces switching losses and thereby improves the spectral performance of the rectifier for less EMI.

4. Summary

A new PFC boost converter with an integrated stand-by flyback converter that can achieve soft-switching of all semiconductor devices in the power stages has been introduced. By using a single magnetic device which is mutually shared by the PFC boost converter and the stand-by flyback converter, boost switch S and flyback switch S_D are turned on with ZVS, auxiliary switch S_1 is turned off with ZCS, and boost diode D is turned off softly using a controlled di/dt rate. As a result, the turn-on switching losses in the boost and flyback switches, the turn-off switching loss in the auxiliary switch, and reverse-recovery-related losses in the boost diode are eliminated, which maximizes the conversion efficiency. The performance of the proposed converter was verified on a 150-kHz, 450-W prototype circuit that was designed to operate from a universal ac-line input and deliver up to 1.2 A at 380-V output voltage by the PFC front end and 2.2 A at 12-V output voltage by the integrated flyback converter. The proposed technique improves the efficiency by approximately 5% at 450 W.

References

- [1] R. Streit, D. Tollik, "High efficiency telecom rectifier using a novel soft-switched boost-based input current shaper," *International Telecommunication Energy Conf. (INTELEC) Proc.*, pp. 720-726, Oct. 1991.
- [2] G. Hua, C.S. Leu, F.C. Lee, "Novel zero-voltage-transition PWM converters," *IEEE Power Electronics Specialists' Conf. (PESC) Rec.*, pp. 55-61, June 1992.
- [3] D.C. Martins, F.J.M. de Seixas, J.A. Brillhante, I. Barbi, "A family of dc-to-dc PWM converters using a new ZVS commutation cell," *IEEE Power Electronics Specialists' Conf. (PESC) Rec.*, pp. 524-530, June 1993.
- [4] J. Bassett, "New, zero voltage switching, high frequency boost converter topology for power factor correction," *International Telecommunication Energy Conf. (INTELEC) Proc.*, pp. 813-820, Oct. 1995.
- [5] C.M.C. Duarte, I. Barbi, "An improved family of ZVS-PWM active-clamping dc-to-dc converters," *IEEE Power Electronics Specialists' Conf. (PESC) Rec.*, pp. 669-675, 1998.
- [6] M.M. Jovanović, "A technique for reducing rectifier reverse-recovery-related losses in high-voltage, high-power boost converters," *IEEE Applied Power Electronics (APEC) Conf. Proc.*, pp. 1000-1007, Mar. 1997.
- [7] Y. Jang, M.M. Jovanović, "A new, soft-switched, high-power-factor boost converter with IGBTs," *International Telecommunication Energy Conf. (INTELEC) Proc.*, Paper 8-3, 1999.
- [8] J.P. Gegner, C.Q. Lee, "Zero-voltage-transition converters using a simple magnetic feedback technique," *IEEE Applied Power Electronics (APEC) Conf. Proc.*, pp. 590-596, 1994.
- [9] N.P. Filho, V.J. Farias, L.C. de Freitas, "A novel family of dc-dc converters using the self-resonance principle," *IEEE Power Electronics Specialists' Conf. (PESC) Rec.*, pp. 1385-1391, 1994.
- [10] G. Moschopoulos, P. Jain, G. Joós, "A novel zero-voltage switched PWM boost converter," *IEEE Power Electronics Specialists' Conf. (PESC) Rec.*, pp. 694-700, 1995.
- [11] J.-H. Kim, D.Y. Lee, H.S. Choi, B.H. Cho, "High performance boost PFP (power factor pre-regulator) with an improved ZVT (Zero Voltage Transition) converter," *IEEE Applied Power Electronics (APEC) Conf. Proc.*, pp. 337-342, 2001.
- [12] I.-Q. Lee, D.Y. Lee, B.H. Cho, "High performance boost pre-regulator with improved zero-voltage-transition (ZVT) converter," *IEEE Power Electronics Specialists' Conf. (PESC) Rec.*, pp. 1691-1696, 2003.
- [13] C.A. Canesin, I. Barbi, "Comparison of experimental losses among six different topologies for a 1.6kW boost converter, using IGBT's," *IEEE Power Electronics Specialists' Conf. (PESC) Rec.*, pp. 1265-1271, 1995.
- [14] D.M. Xu, C. Yang, L. Ma, C. Qiao, Z. Qian, X. He, "A novel single-phase active-clamped pfc converter," *IEEE Applied Power Electronics (APEC) Conf. Proc.*, pp. 266-271, 1997.
- [15] F.T. Wakabayashi, M.J. Bonato, C.A. Canesin, "Novel high-power factor ZCS-PWM preregulators," *IEEE Trans. Industrial Electronics*, vol. 48, no. 2, pp. 322-333, Apr. 2001.
- [16] H.S. Choi, B.H. Cho, "Zero-current-switching (ZCS) power factor pre-regulator (pfp) with reduced conduction losses," *IEEE Applied Power Electronics (APEC) Conf. Proc.*, pp. 962-967, 2002.